Ductile fracture prediction in bulk metal forming using multiscale and continuum damage mechanics models

Mohand OULD OUALI[1], **Madjid ALMANSBA**[2] **and Nacer Eddine HANNACHI**[3]
[1] *Laboratoire Elaboration et Caractérisation des Matériaux et Modélisation – LEC2M. Université Mouloud MAMMERI de Tizi-Ouzou, BP 17 RP, 15 000 Tizi-Ouzou. ALGERIA*
e-mail: m_ouldouali@mail.ummto.dz
[2] *Laboratoire LAMOMS. Université Mouloud MAMMERI de Tizi-Ouzou, BP 17 RP, 15 000 Tizi-Ouzou. ALGERIA*
e-mail: almansbm@mail.ummto.dz
[3] *Laboratoire LAMOMS. Université Mouloud MAMMERI de Tizi-Ouzou, BP 17 RP, 15 000 Tizi-Ouzou. ALGERIA*
e-mail: hannachina@yahoo.fr

Abstract

Two damage models are used in this study to predict ductile fracture of an aluminium alloy during metal forming process. The first one is developed in the framework of phenomenological approach of damage mechanics. The second model is the micromechanical Gurson, Tveergaard and Needleman (GTN) constitutive law describing the three physical mechanisms of ductile fracture: nucleation, growth and coalescence of cavities. In the second model, the voids coalescence onset is modelled using the critical porosity. The value of this material parameter is determined from calibration with experimental tensile test results. These two models have been implemented into the finite elements code Abaqus using the Vectorized User MATerial (VUMAT) subroutine and employed to simulate the forging process of cylindrical and flanged specimens. The confrontation between the predictions of these models and the experimental results shows the capability of these two constitutive laws to predict the evolution forging force. However, the GTN model fails to capture the failure of the two workpieces, which are essentially subjected to compressive loading.

Keywords: forging process, damage mechanics, micromechanical modeling, experiment, porosity, numerical simulation.

1. Introduction

Ductile fracture of metals is today recognized governed by three physical mechanisms: nucleation of initially inexistent voids, growth of theses voids under an appropriated loading and finally coalescence of the neighbouring voids. Several approaches are used to model this phenomenon, generally observed at large deformations over the last three decades. These efforts have been mainly concentrated on modelling this progressive material degradation, namely called material damage. The most used models in metal forming are either phenomenological or micromechanically based. The numerical simulation is generally used to study the workability of materials which can be defined as the degree of deformation that can be supported in a particular metal forming process without generating any undesirable condition, such as cracks, fracture, buckling…

In this paper we introduce some numerical and experimental results obtained from studying axisymmetric forging process. The experimental results concern the response of cylindrical and flanged specimens during metal forming. The numerical aim of this work is to compare two constitutive laws. The first one is developed in the framework of the phenomenological approach, called in this paper the Saanouni and co-workers model [3,33-36,18,19,23]. The second law is the micromechanical Gurson, Tveergaard and Needleman (GTN) model [2,14,15,42,43]. These formulations have been implemented into Abaqus/Explicit finite element package. Both qualitative and quantitative comparison between simulations and experiments results will be done.

2. Experiments

The material used is a commercial aluminium alloy. All the specimens used in this study are machined from one bar with 6m length and 35mm diameter. The mechanical properties of this alloy are measured from tensile tests. These tests are carried out on cylindrical samples standardized in accordance with ISO527-2 standard. The geometry of the tensile specimens is represented in the figure 1. This specimen bar is standardized with respect to the 527-2 standard. We have make choose of the following values: $L_0 = 50mm$, $L = 115mm$, $L_1 = 80mm$, $b_1 = 10mm$, $h = 4mm$, $L_3 = 150mm$ and $b_2 = 20mm$.

The main characteristics of the aluminium alloy obtained during the tensile tests are the Young's modulus $E = 70\,000\,MPa$, the Poisson's ratio $\nu = 0,34$, the yield strength $\sigma_e = 378,34\,MPa$ and the ultimate strength $\sigma_m = 527,39\,MPa$.

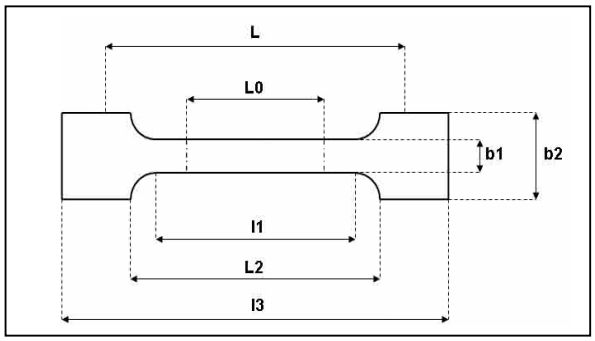

Figure 1: Geometry of the tensile specimen

We show in figures 2 and 3 the microstructures of two samples analyzed after chemical preparation with optical microscopy and cutted respectively in the radial and longitudinal directions. It appear clearly in the figure 3 the formation of sliding bands in the axial direction dues to the bar extrusions effects. These observations comfort the hardenable elastoplastic models choose to simulate the material response. Thos choose is also comforted by stress versus deformation curves obtained form tensile tests.

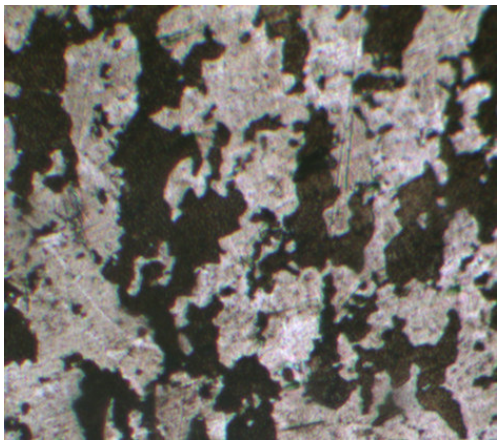

Figure 2: Microstructure of a sample observed in the radial direction after chemical preparation

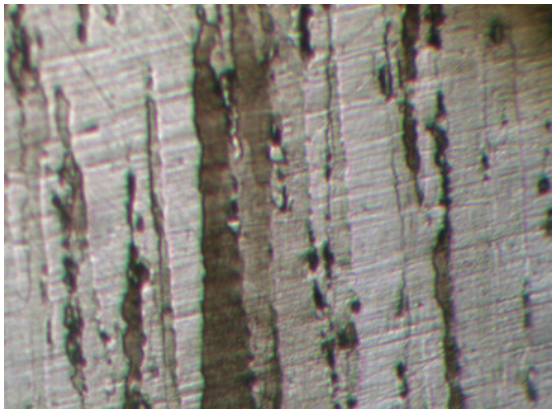

Figure 3: Microstructure of a sample observed in the longitudinal direction after chemical preparation

With the aim of using micromechanical model, the initial porosity of the aluminium alloy is measured in figure 4. the initial porosity f_0 is estimated from the particle void volume fraction f_p using the relation [9,16,27]:

$$f_0 = W_0 f_p \tag{1}$$

where W_0 represents the mean particles shape parameter.

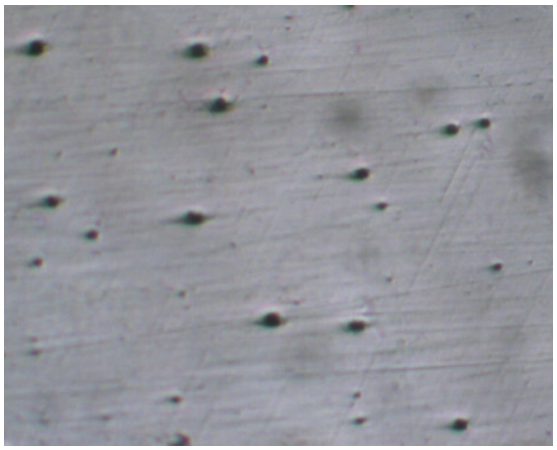

Figure 4: Microstructure of a sample observed in the longitudinal direction before chemical preparation

The workpieces used during metal forming are machined from the same bar. Two shapes are used: cylindrical and flanged types. The tests are carried out in quasi static conditions at room temperature by imposing a length reduction to the pieces.

3. Modeling

3.1. Micromechanical Approach

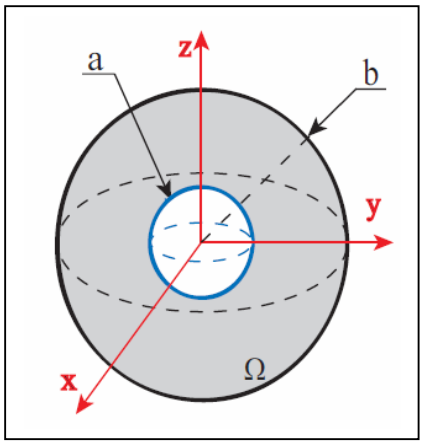

Figure 5: Geometry of the RVE considered in the GTN model (spherical voids)

The so-called Gurson-Tvergaard-Needleman (GTN) model is used to describe ductile fracture of the two aluminium specimens subjected to forging process [14,24,27,42,43]. This

constitutive law is formulated within the framework of homogenization and limit analysis theories. The representative Volume Elementary (RVE) considered is either spherical (Figure 1) or cylindrical containing one cavity of the same shape, and subjected to some asymmetric loadings. The expression of the plastic potential in the case of spherical voids is [14,42,43]:

$$\Phi=\left(\frac{\sigma_{eq}}{\bar{\sigma}}\right)^2+2q_1f^*\cosh\left(\frac{3q_2\sigma_m}{2\bar{\sigma}}\right)-1-\left(q_1f^*\right)^2=0 \tag{2}$$

where σ_{eq}, σ_m and $\bar{\sigma}$ are respectively the von Mises, mean and flow stresses. q_1 and q_2 are coefficient introduced by Tvergaard to take into account namely the interaction between neighbouring cavities. In this study they are assumed depending on the hardening exponent n [32]. f^* is a function establish by Tvergaard and Needleman to simulate the rapid void coalescence at failure:

$$f^*=\begin{cases} f & \text{if } f\le f_c \\ f_c+\delta\left(f-f_c\right) & \text{if } f>f_c \text{ with } \delta=\dfrac{f_u-f_c}{f_F-f_c}\end{cases} \tag{3}$$

f_u is the value of f^* in the plastic potential at zero stress. Taking into account the plastic incompressibility of the matrix, the porosity evolution law which characterizes the damage growth can be written:

$$\dot{f}=\left(1-f\right)\dot{\varepsilon}_{kk} \tag{4}$$

The hardenable behaviour law is obtained by writing the equivalence between the microscopic and macroscopic plastic dissipation as suggested by Gurson [14].

$$\boldsymbol{\sigma}:\dot{\boldsymbol{\varepsilon}}^p=\left(1-f\right)\bar{\sigma}\,\dot{\bar{\varepsilon}}^p \tag{5}$$

where $\dot{\bar{\varepsilon}}^p$ the effective plastic strain rate of the matrix. The isotropic hardening is described by the power law:

$$\frac{\bar{\sigma}}{\sigma_0}=\left(\frac{\varepsilon}{\varepsilon_0}\right)^n \tag{6}$$

σ_0 is the yield stress and ε_0 the strain corresponding to σ_0. With the assumption of normality, the plastic strain increment is in the direction of the outward normal to the yield surface and is related to the rate of the Cauchy stress tensor by

$$\dot{\boldsymbol{\varepsilon}}^p=\frac{1}{\hbar}\left(\frac{\partial\phi}{\partial\boldsymbol{\sigma}}:\dot{\boldsymbol{\sigma}}\right)\frac{\partial\phi}{\partial\boldsymbol{\sigma}} \tag{7}$$

The above constitutive relations have been referred to as GTN model. This model and several of its extensions have been used to predict ductile damage and fracture in metal materials. They reveal clearly in particular the key role of stress triaxiality to the void growth and coalescence. May be on of its important extension concern the incorporation of the cavities shape effects on the mechanical damage of metals is proposed by Gologanu and al. [2,11,26,31]

3.2. Phenomenological approach

The basis idea of the continuum damage mechanics is that the damage variable D represents an average of the effects of the nucleation, growth and coalescence of voids, in a representative volume at the mesoscale, on the load-carrying capacity of the material. The pioneer works on this domain are attributed to Kachanov who introduce a state variable to describe the brittle creep fracture of material [17]. In the eighteen years, Lemaitre and co-workers [20-22] make use of the thermodynamics of irreversible processes and postulate energy potentials to establish state laws and evolution equations of internals variables. Saanouni and co-workers [3,23,33-36] formulated an efficient model describing ductile fracture of metals. This constitutive law is elaborated to describe the elastoplastic behaviour of damageable materials with non-linear hardenings laws. In this model the progressive damage prediction model is a stress based model which assumes that the material progressive degradation can be described by scalar damage variable D. Based on the energy equivalence principle the relation between the effective and applied stress tensors, respectively $\tilde{\boldsymbol{\sigma}}$ and $\boldsymbol{\sigma}$ is:

$$\tilde{\sigma}=\frac{\sigma}{\sqrt{1-D}} \tag{8}$$

The existence of a thermodynamic potential is postulated from which these variables derive. The free energy of Helmholtz is used as thermodynamic potential. This last is assumed depending on the internal and observable variables in the fictitious configuration [20-22,33]. The free energy used by Saanouni and al. is the contribution of an elastic, plastic and due to damage parts [32-36]:

$$\rho\psi=\rho\psi_e\left(\varepsilon^e,D\right)+\rho\psi_p\left(\varepsilon^p,r,D\right)+\rho\psi_d\left(Y,D\right) \tag{9}$$

with:

$$\rho\psi_e\left(\varepsilon^e,D\right)=\frac{1}{2}\varepsilon^e:\hat{\Lambda}\left(D\right):\varepsilon^e \tag{10}$$

$$\rho\psi_p\left(r,D\right)=\frac{1}{2}\tilde{Q}\left(D\right):r^2 \tag{11}$$

The state relations which result from this potential can be written as follow:

$$\sigma=\rho\frac{\partial\psi}{\partial\varepsilon^e}=\tilde{\Lambda}:\varepsilon^e=\left(1-D\right)\Lambda:\varepsilon^e \tag{12}$$

$$R=\rho\frac{\partial\psi}{\partial r}=\tilde{Q}r=\left(1-D\right)Qr \tag{13}$$

$$Y=\rho\frac{\partial\psi}{\partial D}=Y_e+Y_r+Y_D \tag{14}$$

Y is the damage force associated with D.

The following relations deduced from energy equivalence principl, are employed:

$$\tilde{R}=\frac{R}{\sqrt{1-D}} \tag{15}$$

$$\tilde{r}=\sqrt{1-D}\,\mathrm{r} \tag{16}$$

$$\tilde{Q}=\sqrt{1-D}\,\mathrm{Q} \tag{17}$$

The constants $\tilde{Q}$ and Q are respectively the hardening coefficient of the damaged and undamaged material. Y_e, Y_r and Y_D are given by:

$$Y_e = \frac{1}{2}\underline{\underline{\varepsilon}}^e : \frac{\partial \tilde{\Lambda}}{\partial D} : \underline{\underline{\varepsilon}}^e \tag{18}$$

$$Y_r = \frac{1}{2}\frac{\partial \tilde{Q}(D)}{\partial D} r^2 \tag{19}$$

$$Y_D = \frac{1}{(1-D)^\gamma}\frac{S}{s+1}\left[\frac{\langle Y - Y_0\rangle}{S}\right]^{s+1} \tag{20}$$

In order to establish the evolution laws of the internal variables, it's necessary to introduce a dissipation potential F. The expression used by Saanouni and al. [32-36] in the case of an isotropic material hardening is:

$$F = \Phi + \frac{1}{2}\frac{b}{Q}\tilde{R}^2 + \frac{1}{(1-D)^\gamma}\frac{S}{s+1}\left[\frac{\langle Y - Y_0\rangle}{S}\right]^{s+1} \tag{21}$$

where Φ is the von Mises plasticity criterion. This potential allows the complete definition of the plastic deformation, the isotropic hardening and the damage evolution laws:

$$\dot{\varepsilon}^p = \dot{\lambda}\frac{\partial F}{\partial \sigma} = \frac{\dot{\lambda}}{\sqrt{1-D}}\mathbf{n} \tag{22}$$

$$\dot{r} = -\dot{\lambda}\frac{\partial F}{\partial R} = \frac{\dot{\lambda}}{\sqrt{1-D}}\left(1 - b\tilde{r}\right) \tag{23}$$

$$\dot{D} = \dot{\lambda}\frac{\partial F}{\partial Y} = \dot{\lambda}\frac{1}{(1-D)^\beta}\left[\frac{Y - Y_0}{S}\right]^s \tag{24}$$

with:

$$\mathbf{n} = \frac{3}{2}\frac{\mathbf{S}}{\sigma_{eq}} \tag{25}$$

The plastic multiplier $\dot{\lambda}$ is determined by enforcing the coherence condition $\dot{\Phi} = 0$:

$$\frac{\partial \Phi}{\partial \sigma} : (1-D)\Lambda : \dot{\varepsilon} - \dot{\lambda}\, H = 0 \tag{26}$$

where H is the elastoplastic modulus:

$$H = h + \frac{3}{2}\frac{E}{1+\nu} + \frac{3}{2}\frac{Y^*}{(1-D)^{\frac{3}{2}}}\frac{S : \tilde{\sigma}}{\sigma_{eq}} \tag{27}$$

and

$$\mathrm{h} = \mathrm{Q} - \mathrm{b}\tilde{\mathrm{R}} - \frac{\mathrm{Y}^*}{1-\mathrm{D}}\left(\tilde{\mathrm{R}} + \frac{\sigma_\mathrm{y}}{2}\right) \tag{28}$$

$$\mathrm{Y}^* = \frac{\partial \mathrm{F}}{\partial \mathrm{Y}} = \frac{1}{(1-\mathrm{D})^\beta}\left[\frac{\mathrm{Y}}{\mathrm{S}}\right]^\mathrm{s} \tag{29}$$

β, S and s are material parameters which can depend on the actual temperature.

4. Implementation

The two models discussed in the previous section have been implemented into ABAQUS/Explicit solver through a Vectorized User MATerial (VUMAT) subroutine [1,37]. Abaqus is a displacement based finite element code which allocates the resolution of the mechanical equilibrium equation by both spatial and time discretizations [1]. So, the weak form of the virtual principal work can be written as follow [1,27,28]:

$$\boldsymbol{M}\ddot{\boldsymbol{u}} + \boldsymbol{F}_{int} - \boldsymbol{F}_{ext} = 0 \tag{30}$$

where the consistent mass matrix $\boldsymbol{M}$, the internal and external forces vectors $\boldsymbol{F}_{int}$ and $\boldsymbol{F}_{ext}$ respectively are the assemblies of the elementary ones calculated for each element by using the classical nodal approximation. The resolution of the above equation according to the dynamic explicit scheme is possible by first calculating the acceleration vector:

$$\ddot{\boldsymbol{u}} = \boldsymbol{M}^{-1}\left(\boldsymbol{F}_{int} - \boldsymbol{F}_{ext}\right) \tag{31}$$

Then the speed $\dot{\boldsymbol{u}}$ and displacement $\boldsymbol{u}$ vectors are evaluated at each increment:

$$\dot{\boldsymbol{u}}_{n+\frac{1}{2}} = \dot{\boldsymbol{u}}_{n-\frac{1}{2}} + \frac{\Delta t_{n+1} + \Delta t_n}{2}\ddot{\boldsymbol{u}} \tag{32}$$

$$\boldsymbol{u}_{n+1} = \boldsymbol{u}_n + \Delta t_{n+1}\dot{\boldsymbol{u}}_{n+\frac{1}{2}} \tag{33}$$

It appears in the equations 31-33 that the estimation of the displacement vector can be done by calculating the internal force vector which depends on the actual stress tensor. So, this tensor should be calculated at every increment using the constitutive law considered.

The numerical scheme adopted to implement the two models described in the previous section is the "elastic predictor-plastic correction" one. In the case of the Saanouni and co-workers model the plastic correction is carried out using the radial return method proposed by Simo and Ortiz [17,38,39]. After some developments, the equation set to resolve can be reduced to [23,18,34]:

$$\begin{cases} \Phi(\Delta\lambda, D) & = \left\| \boldsymbol{S}^{*}_{n+1} \right\| - \dfrac{2}{3}\left[\dfrac{Q}{1+b\Delta\lambda}\left(r_n + \dfrac{\Delta\lambda}{\sqrt{1-D_{n+1}}} \right) \right] \\ & \quad + \dfrac{1}{\sqrt{1-D_{n+1}}}\sigma_0 + 3G\dfrac{1}{\sqrt{1-D_{n+1}}}\Delta\lambda \\ g\left(\Delta\lambda, D\right) & = D_{n+1} - D_n - \Delta\lambda \hat{Y}_{n+1} \end{cases} \quad (34)$$

where $\boldsymbol{S}$ is the deviator part of $\boldsymbol{\sigma}$. The set of two equations (34) can be solved by applying the Newton-Raphson method. This leads to the following system of two equations with two unknowns $\left(\Delta\lambda, D\right)$ which can solved iteratively at each increment:

$$\begin{cases} \Phi^{i} + \left[\dfrac{\partial \Phi}{\partial \Delta\lambda} \right]^{i} \delta\lambda + \left[\dfrac{\partial \Phi}{\partial D_{n+1}} \right]^{i} \delta D = 0 \\ g^{i} + \left[\dfrac{\partial g}{\partial \Delta\lambda} \right]^{i} \delta\lambda + \left[\dfrac{\partial g}{\partial D_{n+1}} \right]^{i} \delta D = 0 \end{cases} \quad (35)$$

The GTN model is implemented following the Aravas's algorithm [4,5,13]. This technique is based on the decomposition of the stress tensor into its hydrostatic σ_m and deviator parts σ_{eq} and the plastic strain increment tensor $\Delta\boldsymbol{\varepsilon}^{p}$ into its volumetric and deviator parts:

$$\boldsymbol{\sigma} = \sigma_m \mathbf{1} + \frac{2}{3}\sigma_{eq}\mathbf{n} \quad (36)$$

$$\Delta\boldsymbol{\varepsilon}^{p} = \frac{2}{3}\Delta\varepsilon_{\mathrm{p}}\mathbf{1} + \Delta\varepsilon_{q}\mathbf{n} \quad (37)$$

$\Delta\varepsilon_{\mathrm{p}}$ and $\Delta\varepsilon_{q}$ are used by Aravas as primary variables to permit the reduction of the unknowns number. The system to be numerically integrated is reduced to two non-linear equations:

$$\Delta\varepsilon_{\mathrm{p}}\frac{\partial \Phi}{\partial \sigma_{eq}} + \Delta\varepsilon_{q}\frac{\partial \Phi}{\partial \sigma_{m}} = 0 \quad (38)$$

$$\Phi\left(\boldsymbol{\sigma}, f, \bar{\sigma}\right) = 0 \quad (39)$$

Details of these two procedures can be found in the appendix and/or in the references [4,19,27,34].

5. Results and discussion

The cylindrical and flanged specimens with initial lengths $l_0 = 35\,mm$ (see figure 6) are positioned between two rigid tools. This rigidity assumption is reasonable because of the stiffness and the yield strength of the aluminium alloy are significantly lowers than those of the pieces. One of the rigid tools is maintained fixed and the other is affected with a displacement of $10mm$ under quasi-static condition $\left(5mm/mn\right)$. The halves of the two specimens are meshed with axisymmetric solid element with reduced integration CAXR: 248 for the flanged and 300 for the cylindrical pieces.

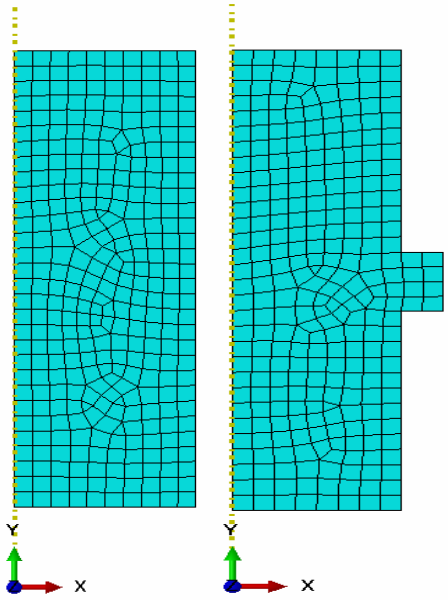

Figure 6: Shape of the two workpieces used in metal forming (cylindrical in the left, flanged in the right)

The mains damage and hardening material parameters are calculated by calibrating the tensile experimental results with numerical predictions of the two models presented above. However, the initial material porosity f_0 is quantified with measure of the particles rate in the plane perpendicular to the axis of the specimen (figure 4). The main parameters obtained are recapitulated in table 1:

Table 1: Material parameters of the GTN and Saanouni and al. models

Models	Material parameters				
GTN model	$f_0 = 9,91.10^{-5}$	$f_c = 11,97.10^{-5}$	$f_F = 0,001$	$n = 0,1$	
Saanouni and al. model	$S = 20$	$s = 0,1$	$Y_0 = 6$	$Q = 2581$	$b = 15$

As mentioned above, the material parameters presented in table1 are obtained by comparisons between the numerical and experimental curves of tensile tests. The good concordance of the three curves observed in figure 7 indicates the validity of the identification procedure.

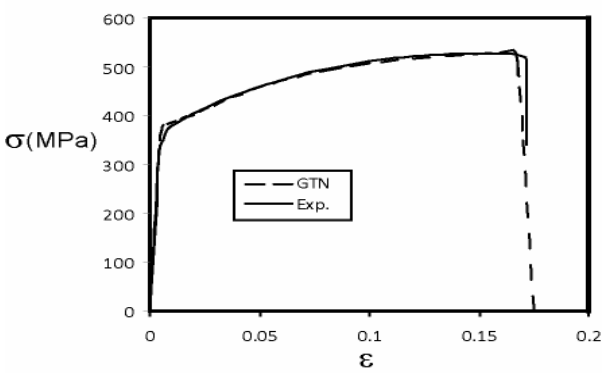

Figure 7: Determination of the material parameters of the GTN model by numerical calibration.

In order to asses the capability of theses two models to describe the material response during the forming process, we show in the figures 8 and 9 comparison between the forging forces calculated numerically and experimentally versus the lengths reductions of the cylindrical and flanged specimens.

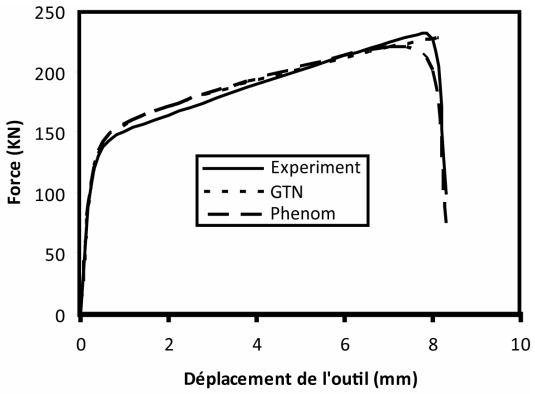

Figure 8: Forging force-length reduction (cylindrical specimen).

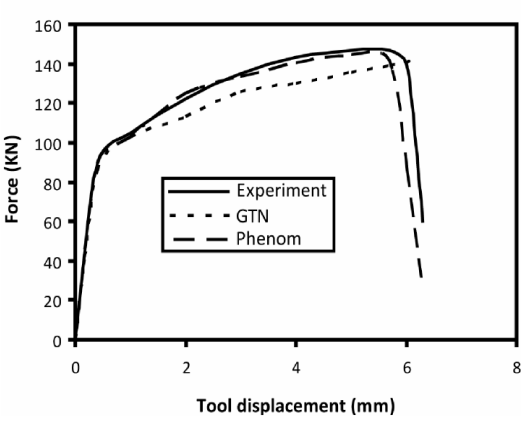

Figure 9: Forging force-length reduction (flanged specimen).

Good agreements were also found between experimental and numerical results during the force evolution stage. However the GTN model fails to capture the final workpieces failure during the two tests. This situation can be explained by the fact that in this model, the onset of coalescence is governed by the critical porosity. The value of this material parameter is determined by calibration with tensile tests, whereas the loadings during the forming tests are effectively compressive.

Figure 10 represents the distribution of the damage variable calculated numerically with the Saanouni and co-workers model and a photo at the fracture of a specimen subjected experimentally to forging process. The damage zone is also correctly predicted by this model which comforts the previous results. In the case of simulations with the GTN constitutive law, the results show at the end of the forging operation concentration and increase of the plastic strain in approximately the damage band, however the values of the porosity are near the initial porosity.

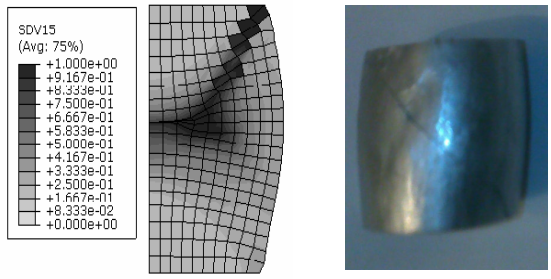

Figure 10: Distribution of the damage variable . Comparison with experimental results

6. Conclusion and perspectives

In this work two mechanical damage models are used to describe ductile fracture of an aluminium alloy during metal forming. The first one is the micromechanical Gurson, Tveergaard and Needleman (GTN) model describing the three physical mechanisms of ductile fracture: nucleation, growth and coalescence of cavities. The second constitutive law is developed in the framework of phenomenological approach of damage mechanics. The basis idea of this approach is that the damage variable represents an average of the effects of the nucleation, growth and coalescence of voids on the load-carrying capacity of the material. Both theoretical and numerical aspects are presented. The material parameters identification procedure of the two models is clearly explained. The predictions of these models were compared with experimental results measured from cylindrical and flanged specimens subjected to forging process. The results show the capabilities of the phenomenological and micromechanical models to describe successfully the forging force evolution. However the GTN model doesn't predict the two specimen's failures. As explained, this situation is due to the coalescence onset criterion used.

Consequently, as a perspective of this work it's important to envisage coupling the GTN micromechanically-based model with a criterion which may predict ductile fracture of material subjected to compressive loadings. Many ductile criteria are proposed in the literature: Thomason, Freudenthal, Oyane… [10,40,41,26,28], however one should keep in mind the micromechanical origin of the GTN which restrain considerably our choose. So, one way which can be explored is the extension

of an existing micromechanical criterion to take into account material rupture under compressive loading.

Appendix 1

Implementation of the Saanouni and coworkers model

The plastic correction consists to resolve the system:

$$\begin{cases} g_\varepsilon = \Delta\underline{\varepsilon}^p - \Delta\lambda_p \dfrac{\underline{n}_{n+1}}{\sqrt{1-D_{n+1}}} = 0 \\ g_r = \Delta r - \dfrac{\Delta\lambda_p}{\sqrt{1-D_{n+1}}}\left(1+b\tilde{r}\right) = 0 \\ g_D = \Delta D - \Delta\lambda \hat{Y}^*_{n+1} = 0 \\ h = \underline{\sigma}_{n+1} - (1-D_{n+1})\underline{\underline{\Lambda}} : \left(\underline{\varepsilon}_{n+1} - \underline{\varepsilon}^p_{n+1}\right) = 0 \end{cases} \quad \text{(A1)}$$

This is due by considering firstly the deviator tensor:

$$\underline{S}_{n+1} = (1-D_{n+1})\underline{S}^*_{n+1} - 2G\sqrt{1-D_{n+1}}\Delta\lambda\underline{n}_{n+1} \quad \text{(A2)}$$

where

$$R_{n+1} = (1-D_{n+1})\frac{Q}{1+b\Delta\lambda}(r_n + \frac{\Delta\lambda}{\sqrt{1-D_{n+1}}}) \quad \text{(A3)}$$

$$\underline{D}_{n+1} = D_n + \Delta\lambda\left[\frac{Y-Y_0}{S}\right]^s \frac{1}{(1-D_n)} \quad \text{(A4)}$$

Simo et Taylor [39] proposed the procedure to reduce the system (A1) to two equations with two unknowns by multiplying the the tensor $\mathbf{n}$ with the plastic criterion:

$$f_{n+1}(\underline{\sigma}_{n+1}, \underline{R}_{n+1}, Y_{n+1}, D_{n+1}) = J_2(\underline{\sigma}_{n+1}) - R_{n+1} - \sqrt{1-D_{n+1}}\sigma_y = 0 \quad \text{(A5)}$$

After some development we get the expression:

$$\underline{S}^*_{n+1} = \frac{2}{3}\frac{1}{(1-D_{n+1})}\begin{bmatrix} R_{n+1} + \sqrt{1-D_{n+1}}\sigma_y \\ +3G\sqrt{1-D_{n+1}}\Delta\lambda \end{bmatrix}\underline{n}_{n+1} \quad \text{(A6)}$$

$$\left\|\underline{S}^*_{n+1}\right\| = \frac{2}{3}\frac{1}{(1-D_{n+1})}\begin{bmatrix} R_{n+1} + \sqrt{1-D_{n+1}}\sigma_y \\ +3G\sqrt{1-D_{n+1}}\Delta\lambda \end{bmatrix} \quad \text{(A7)}$$

In the last equation, we have replaced the unknown tensor $\mathbf{n}$ with par $\boldsymbol{S}^*_{n+1}$ which depends only on $\Delta\lambda$.

$$\begin{cases} \Phi(\Delta\lambda, D) = \left\|\boldsymbol{S}^*_{n+1}\right\| - \dfrac{2}{3}\left[\dfrac{Q}{1+b\Delta\lambda}\left(r_n + \dfrac{\Delta\lambda}{\sqrt{1-D_{n+1}}}\right) + \dfrac{1}{\sqrt{1-D_{n+1}}}\sigma_0 + 3G\dfrac{1}{\sqrt{1-D_{n+1}}}\Delta\lambda\right] \\ g\left(\Delta\lambda, D\right) = D_{n+1} - D_n - \Delta\lambda\hat{Y}_{n+1} \end{cases} \quad \text{(A8)}$$

Finally the non linearity of the entire problem is restrained to two unknowns $(\Delta\lambda, D_{n+1})$.

Acknowledgement. The second author would like to express its profound gratitude to the Professeur K. SAANOUNI for helpful discussion and its disponibility during it's long stage at the University of Troyes (France).

References

[1] ABAQUS (2005) Version 6.5.1. HKS, Providence.

[2]Aberkane Méziane and Ould Ouali Mohand. Fracture characterization of ST37-2 thin metal sheet with experimental and numerical methods. Key Engineering Materials, Trans Tech Publications. Vol. 473, pp 396-403, 2011.

[3] M. Almansba, K. Saanouni, N. E. Hannachi, Isotropic Elastoplasticity Fully Coupled with Non-Local Damage, *Journal of Engineering*, 2(6), pp. 420-431, 2010

[4]N. Aravas. On the numerical integration of a class of pressure-dependent plasticity models. International Journal for Numerical Methods in Engineering, 24 :1395-1416, 1987.

[5] N. Aravas and P. Ponte Castañeda. Numerical methods for porous metals with deformation-induced anisotropy. Comput. Methods Appl. Mech. Engrg., 193: 3767-3805,

[6] Benzerga, A. A. and Besson, J., "Plastic potentials for anisotropic porous solids," European Journal of Mechanics, 20A, 397-434; 2001

[7] Benzerga AA, Besson J, Batisse R, Pineau A, Synergistic effects of plastic anisotropy and void coalescence on fracture mode in plane strain. Model. Simul. Mater. Sci. Eng 10:73–102, 2002.

[8] A.A. Benzerga, J. Besson, and A. Pineau. Anisotropic ductile fracture, part ii : theory. Acta Materialia, 52, 2004.

[9] Bethmont M, Rousselier G, Deuesa G, Batisse R (1987) Ductile fracture analysis by means of a local approach. In: 9th int. conf. on structural mechanics in reactor technology, SMIRT9, Lausannne, August 1987, pp 131–141

[10]F. A. Freudenthal, *The Inelastic Behaviour of Solids.* Wiley, New York (1950).

[11] M. Gologanu, J.-B. Leblond, and J. Devaux. Recent extensions of Gurson's model for porous ductile metals, pages 61-130. CISM Lectures Series, Springer, New-York, New York, 1997.

[12] Gouveia BPP, Rodrigues JMC, Martins PAF. Fracture predicting in bulk metal forming. International Journal of Mechanical Sciences 1996; pp. 38:361–72.

[13] Govindarajan RM, Aravas N (1995) Pressure-dependent plasticity models: loading-unloading criteria and the consistent linearization of an integration algorithm. Commun Numer Methods Eng 11:339–345

[14] A.L. Gurson. Continuum theory of ductile rupture by void nucleation and growth: Part i- yield criteria and _ow rules for porous ductile media. ASME J. Engineering Materials Technology, 99 :2-15, 1977.

[15] Hao S, Brocks W (1997) The gurson-tvergaard-needleman model for rate and temperature-dependent materials with isotropic and kinematic hardening. Comput Mech 20:34–40

[16] Huber G, Brechet Y, Pardoen T (2005) Predictive model forvoid nucleation and void growth controlled ductility in quasieutetic cast aluminium alloys. Acta Mater 53:2739–2749

[17] L.M. Kachanov, On the time to failure under creep conditions, *Izv. Akad. Nauk SSR, Otd. Tekhn. Nauk* 8, pp. 26–31, 1958.

[18] Mourad Khelifa, Khémais Saanouni and Abel Cherouat. Prévision de l'endommagement ductile. Application à l'emboutissage de tôles minces. Mécanique & Industries 7, 465-473, 2006.

[19] M. Khelifa, H. Badreddine, N. Belamri, M.A. Gahbiche, K. Saanouni, A. Cherouat and A. Dogui, Effect of anisotropic plastic flow on the ductile damage evolution in hydrobulging test of thin sheet metal, *Int J Forming Process* **8** (2) (2005), pp. 271–289

[20] Lemaitre J, Chaboche JL (1985) Mécanique des matériaux solides. Dunod, Paris

[21] J. Lemaitre, A continuous damage mechanics model for ductile fracture, *J. Engrg. Mat. Tech., Trans. ASME*, 107, pp. 83–89, 1985.

[22]Lemaitre J., *A Course on Damage Mechanics*, Springer-Verlag, 1996.

[23] P. Lestriez, K. Saanouni, J.F. Mariage and J.F. Cherouat, Numerical prediction of damage in metal forming process including thermal effects, *Int J Damage Mech* **13** (1) (2004), pp. 59–80

[24] Needleman A, Tvergaard V (1991) An analysis of dynamic ductile crack growth in a double edge cracked specimen. Int. J Fract 49:41–67

[25]ORTIZ M. and Simo J.C. An analysis of a new class of integration algorithms for elastoplastic constitutives relations, Int. J. Numer. Meth. Eng., vol 23, pp.353-366, 1986

[26]M. Ould Ouali. Approche micromécanique de la rupture ductile dans les procédés de mise en forme des matériaux. Prise en compte de l'effet de forme des cavités. PhD thesis, Université de Reims Champagne-Ardenne, April 20, 2007.

[27]Ould Ouali M. and Aberkane M., Micromechanical modeling of the rolling of a A1050P aluminum sheet, *Int. J. of Material Forming*, 2(1), pp. 25-36, 2009.

[28]M. Oyane, Criteria of ductile fracture strain. *Bull. JSME* 15. 1507 (1972).

[29] Pardoen T, Hutchinson JW (2000) An extended model for void growth and coalescence. J Mech Phys Solids 48:2467–2512

[30] T. Pardoen and J.W. Hutchinson. Micromechanical-based model for trends in toughness of ductile metals. Acta Materialia, 51 :133-148, 2003.

[31] Leblond J.-B., Perrin G. and Devaux J.B. An improved Gurson-type model for hardenable ductile metals. J. Mech. Phys. Solids, 14: pp.499-527, 1995

[32] Ragab A.R., Prediction of ductile fracture in axisymmetric tension by void coalescence, International Journal of Fracture 105: pp. 391-409, 2000

[33] Saanouni, K., Forster C. and Ben Hatira F., On the Anelastic Flow with Damage, *Int. J. of Damage Mechanics*, 3, pp. 140-169, 1994.

[34] Saanouni K., Nesnas K. and Hammi Y. *Damage modelling in metal forming processes*, Int. J. of Damage Mechanics, Vol 9, N°3, pp 196-240, July 2000.

[35] Saanouni K, Chaboche J-L. Computational damage mechanics. In: Milne I, Ritchie RO, Karihaloo B, editors. Comprehencive structural integrity. de Borst R, Mang HA, editors. Application to metal forming, numerical and computational methods, vol. 3, 2003, ISBN:0-08-043749-4 (Chapter 7).

[36] Saanouni K, Mariage JF, Cherouat A, Lestriez P (2004), Numerical prediction of discontinuous central bursting in axisymmetric forward extrusion by continuum damage mechanics. Comput Struct 82(27):2309–2332

[37] Larbi Siad, Mohand Ould Ouali, and Anouar Bennabes. Comparison of explicit and implicit finite element simulations of void growth and coalescence in porous ductile materials. Materials and Design., 29(2) :319-329, 2008.

[38] Simo J.C. and ORTIZ M. A unified approach to finite deformation elastoplastic analysis based on the use of hypoelastic constitutive equations. Appl. Mech. Eng., vol 49, pp.221-245, 1984

[39] SIMO, J. C. et TAYLOR, R. L., «Computational inelasticity». Springer New York, 1998.

[40] Thomason PF (1985) A three-dimensionel model for ductile fracture by the growth and coalescence of microvoids. Acta Metall 33(6):1087–

[41] 1095P.F. Thomason. Ductile fracture of Metals. Pergamon Press, Oxford, 1990.

[42] Tvergaard V (1981) Influence of voids on shear bands instabilities under plane strain conditions. Int J Fract 17: 389–407

[43] V. Tvergaard and A. Needleman. Analysis of the cup-cone fracture in a round tensile bar. Acta Metallurgica, 32 :157-169, 1984.